Supporting Information

Polyelectrolyte Multilayer Assisted Fabrication of p-Cu_2S/n-CdS Nano-heterostructure Thin Films Phototransistor

Ramphal Sharma,[1,2*†] Gangri Cai,[2,3†] Dipak V. Shinde,[2] Supriya A. Patil,[2] Shaheed Shaikh,[1] Anil Vithal Ghule,[2] Rajaram S. Mane[2] and Sung-Hwan Han[2*†]

[1]Thin Film and Nanotechnology Laboratory, Department of Physics, Dr. Babasaheb Ambedkar Marathwada University, Aurangabad 431004 (India)

[2]Inorganic-Nanomaterials Laboratory, Department of Chemistry, Hanyang University, Sungdong-Ku, Haengdang-dong 17, Seoul 133-791 (South Korea)

[3]Department of Applied Chemistry, Tianjin University of Technology, Tianjin 300384, People's Republic of China.

[†]These authors contributed equally to this work.

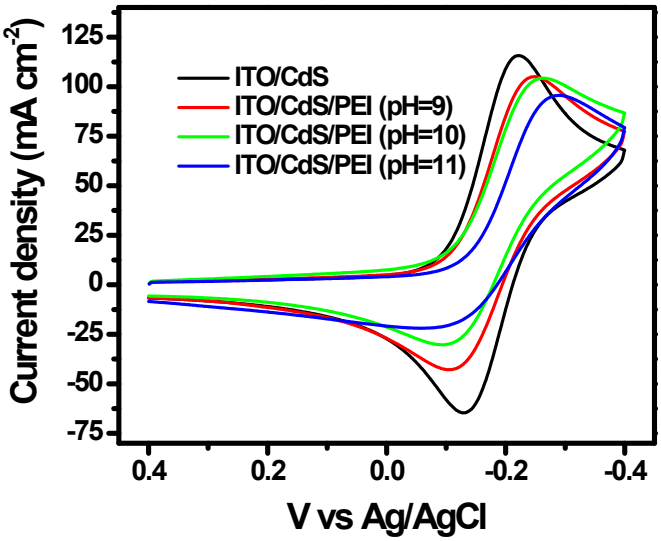

Figure S1a. Cyclic-voltammograms obtained using $Fe(CN)_6^{3-}$ molecules and ITO/CdS/PEI electrode for understanding the best pH condition for preventing cation permeability and/or exchange during the Cu_2S deposition by varying pH values from 9 to11. The cyclic voltametry *(C-V)* study was performed using anionic $Fe(CN)_6^{3-}$ and cationic $Ru(NH_3)_6^{3+}$, redox probe molecules,[1, 2] for ion-permeability test.[3] The ion-permeability is controlled by charge density of the polyelectrolyte layer.[1] The charge density is influenced by the amount of NH_2 groups, which can be modified by film thickness at the same pH condition by controlling the charge density using different dipping conditions.[1, 2] The *C-V* curves as shown in Fig. S1a were recorded with ITO/CdS/PEI electrode samples maintained at varying pH from 9 to 11 to optimize the best condition for preventing ion (cation) permeability during Cu_2S deposition onto the pre-deposited CdS layer. The successive shift and decrease in redox current of cationic probe with increase in pH of the solution to ~11 justifies effective blocking of the cations even with the single layer of PEI. The results indicate that the experiments performed at pH ~11 showed better blocking effect, prohibiting the exchange of cations across the protecting polyelectrolyte layer.

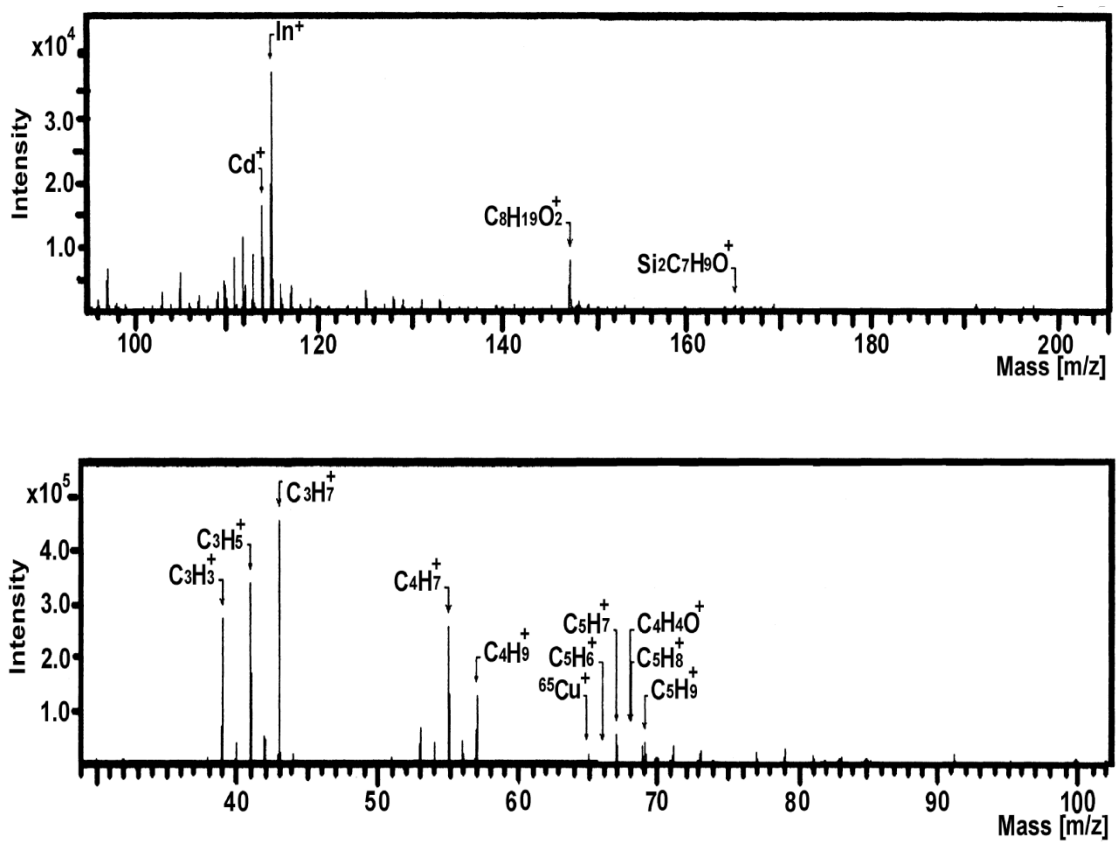

Figure S1b: The TOF-SIMS cations spectrum of 200^0C annealed 1h in air of *p*-Cu_2S/*n*-CdS thin films.

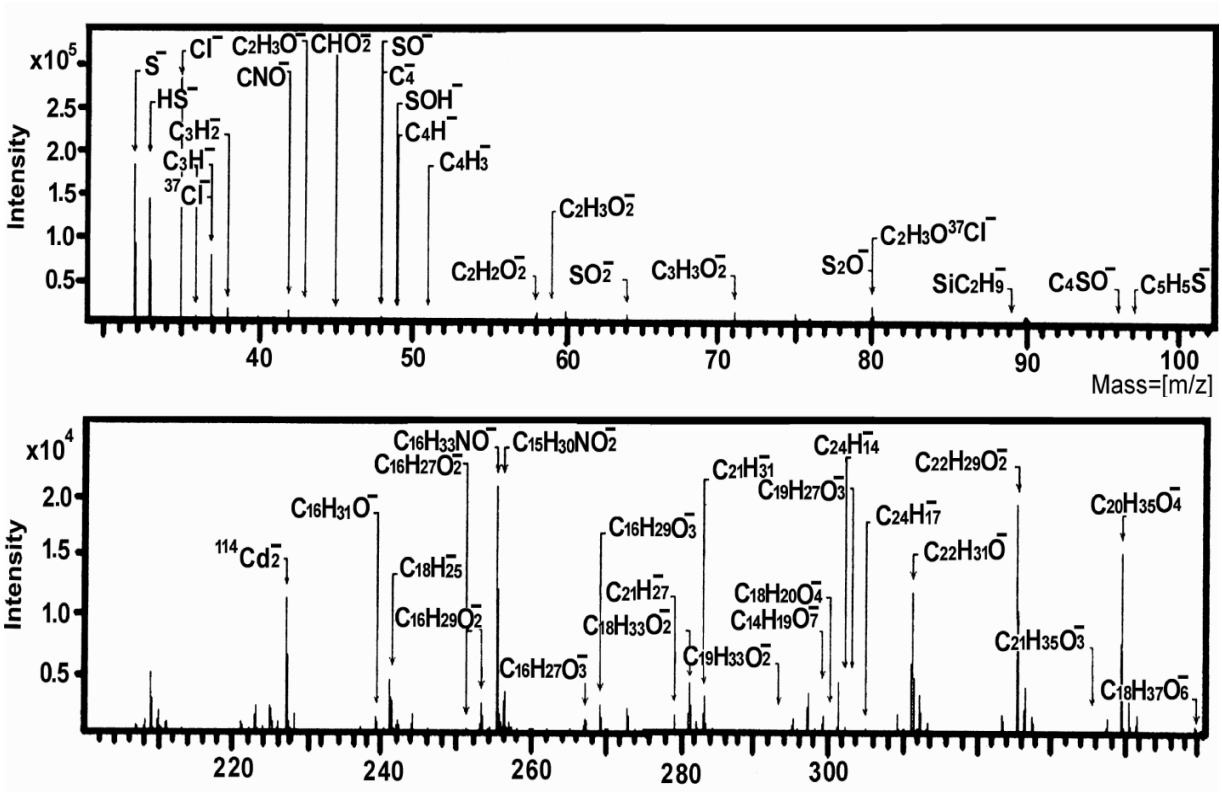

Figure S1c : The TOF-SIMS anion spectrum of 200 ^{0}C annealed 1h in air of *p*-Cu_2S/*n*-CdS thin film.

The sandwich layers (PEI/PAA)$_{1.5}$ of the p-Cu_2S/n-CdS thin films annealed at 200^0 1h in air are analyzed using cations and anions spectrums of TOF-SIMS spectroscopy in the imaging modes analysis. The emitted secondary ions are extracted into the TOF analyzer by applying a high voltage potential between the p-Cu_2S/n-CdS thin films surface and the mass analyzer. TOF-SIMS spectra are generated using a pulsed primary ion source (very short pulses of <1 ns). Secondary ions travel through the TOF analyzer with different velocities, depending on their mass to charge ratio (ke =½mv ^{2}). For each primary ion pulse, a full mass spectrum is obtained by measuring the arrival times of the secondary ions at the detector and performing a simple time to mass conversion and the cations and anions spectrums were obtained respectively. From the TOF-SIMS cations spectrums Fig. S1 b and anions spectrum Fig.1c study, it can be confired that cantions and anions of PEI/PAA are presented in sandwich of *p*-Cu_2S/*n*-CdS thin film for the protection of cation exchange.

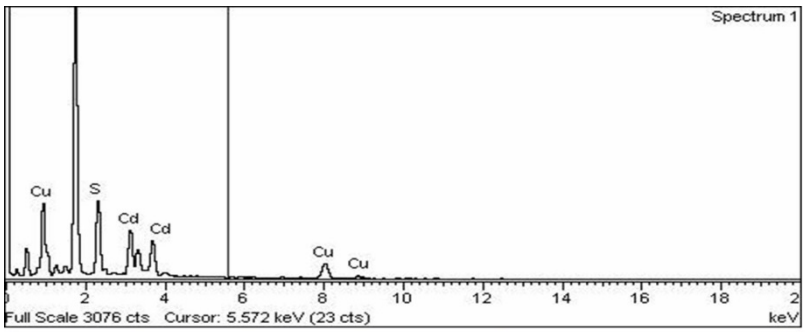

Element	App Conc.	Intensity Corrn.	Weight%	Weight% Sigma	Atomic%
Cd L	9.10	0.7999	11.36	0.37	25.45
Cu K	6.94	0.9641	7.20	0.40	28.54
S K	5.31	0.9074	5.86	0.13	46.01
Totals			24.43		

Figure S2. Energy dispersive X-ray analysis spectra obtained from Cu_2S/CdS thin-film and corresponding quantitative elemental analysis data.

The SEM images were obtained from the CdS, Cu_2S and Cu_2S/CdS thin-film heterojunction. SEM image of Cu_2S/CdS thin-film heterojunction show smooth Cu_2S film surface with Cu_2S nanoparticles covering the entire CdS layer (main text Fig. 1b). Quantitative elemental analysis of the Cu_2S/CdS thin-film heterojunction from the EDS spectra showed the presence of Cd (25.45 %), Cu (28.54 %) and S (46.01 %) elements. This further justifies the use of multiple polyethyleneimine (PEI) and polyacrylic acid (PAA) (PEI/PAA) polyelectrolyte layers for effective protection of cation exchange reaction on the CdS thin-film surface, supporting the formation of Cu_2S/CdS chalcogenide semiconductor heterojunction.

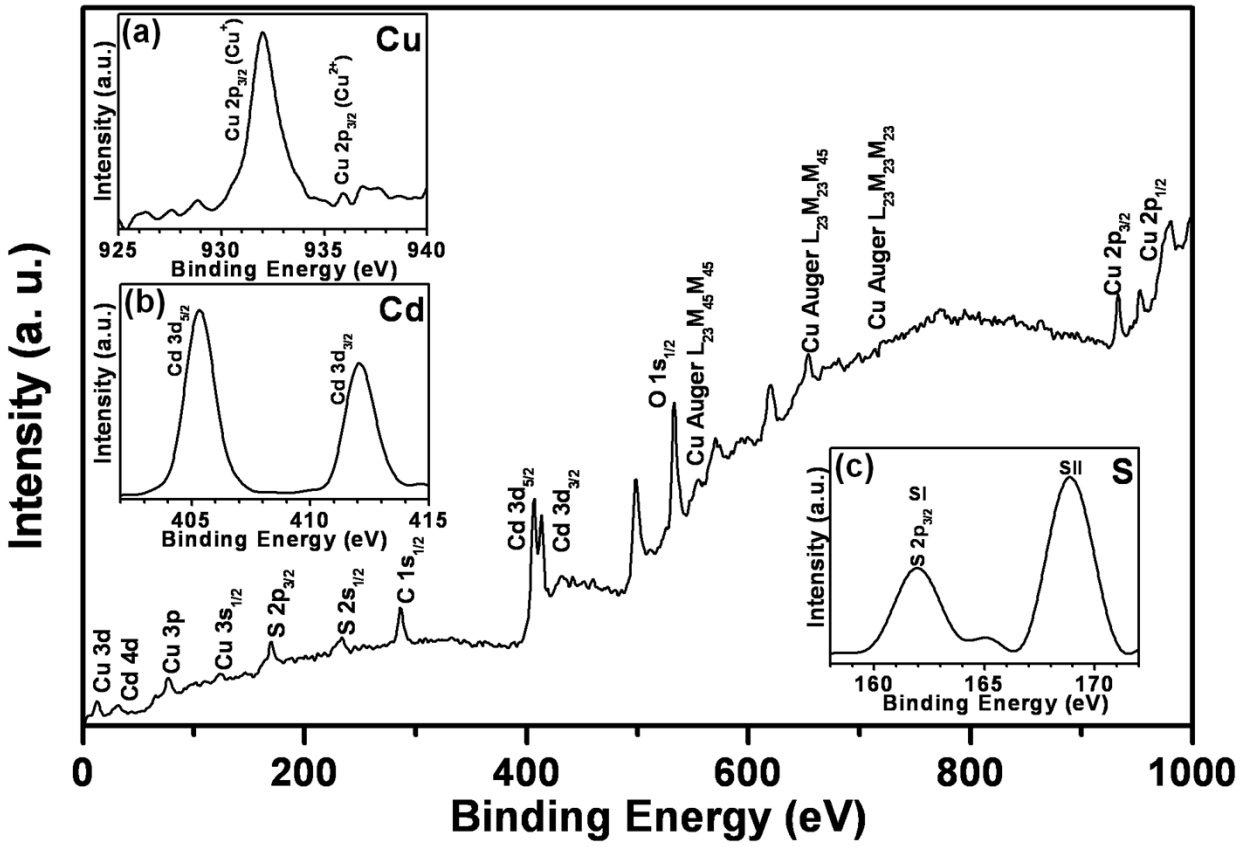

Figure S3. XPS surface survey spectrum obtained from Cu_2S/CdS thin-film heterojunction. Insets show high resolution XPS spectra of characteristic peaks of (a) Cu, (b) Cd, and (c) S.

The XPS measurements have been carried out to obtain the composition and chemical bonding between the elements within the annealed Cu_2S/CdS thin-film heterojunction. A survey spectrum is presented in Fig. S3. The spectrum clearly shows the valence and core level binding energy peaks of Cu, Cd, and S elements, indicating their involvement in the film composition, and elements C (used as reference) and O as impurity. The presence of oxygen in the film is likely due to annealing of the film in air atmosphere. No binding energy peaks characteristic of Cl or Na originating from the reactants were observed, which indicates that the annealed thin films are possibly free from impurities. High-resolution XPS spectra characteristic of Cu 2p, Cd 3d, and S 2p were used to determine the valence state and atomic ratio are shown as insets Figs. S3a, S3b and S3c, respectively. Fig. S3a shows the Cu 2p core level spectrum; it is observed from the spectrum that the values of the binding energies for Cu

$2p_{3/2}$ and Cu $2p_{1/2}$ are quite consistent with the literature values.[2, 4] The full width at half maximum (FWHM) for Cu $2p_{3/2}$ peak is 1.89 eV, which is in good agreement with the literature values for Cu^{+} ions.[5] In addition, the Cu $2p_{3/2}$ satellite peak of low intensity Cu^{2+}, which is usually centered at 935.8 eV also appears in the spectrum.[6] Therefore, it can be concluded that large number of Cu^{+} ions exists in the sample than that of Cu^{2+} ions. Fig. S3b represents the typical Cd 3d core level spectrum, showing strong peaks at 405.3 and 412.1 eV corresponding to the characteristic Cd $3d_{5/2}$ and Cd $3d_{5/2}$ binding energy of Cd element. The S 2p core level spectrum (Fig. S3c) shows two peaks, one at 161.8 eV corresponding to S from Cu-S and the other at 164.8 eV corresponding to S from Cd-S.[7] The lower binding energy peak at SI (161.8 to 164.8 eV) is an indicative of metal sulphide, while the other peak at SII (168.9 eV) has been assigned to more oxidized (metal sulphate) from the sulphur.[8]

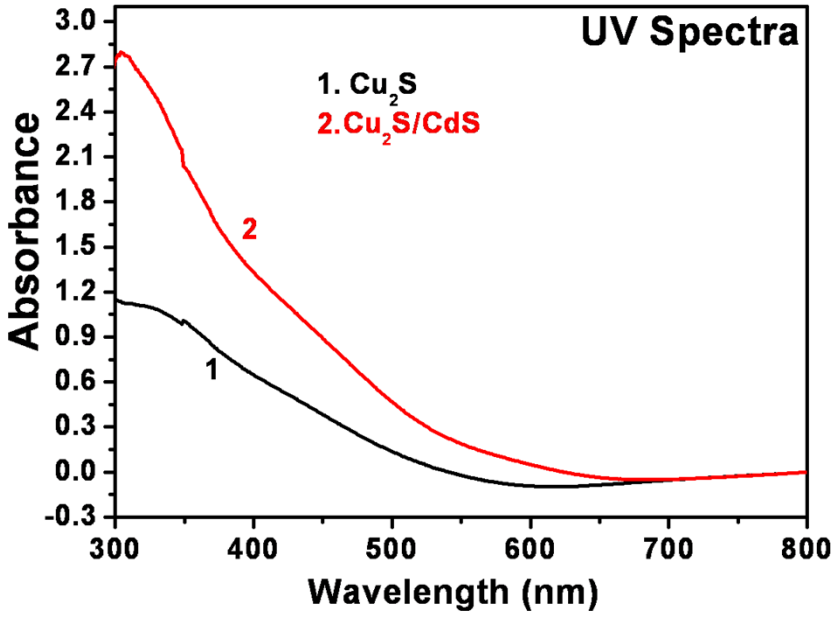

Figure S4. UV-visible spectra obtained from Cu_2S (curve 1) and Cu_2S/CdS (curve 2) thin films.

UV-vis absorption and photoluminescence (PL) measurements were performed to study the effect of (PEI/PAA)n multilayer in protecting the ion exchange reactions during the growth of Cu_2S film and the optical properties. UV visible spectra obtained from the Cu_2S thin-film (curve 1) and Cu_2S/CdS thin-

film heterojunction (curve 2) in the range from 300 to 800 nm are shown in Fig. S4. Curve 2 shows increased UV-vis absorption in the visible region (400 to 700 nm) with prominent tailing effect extending to the red side, when compared to plain Cu_2S film (curve 1) indicating excitonic absorption structure. To investigate the contribution of Cu_2S to the observed absorption, UV-vis absorption spectra of Cu_2S film alone is recorded as shown in Fig. S4 (curve 1). The UV-vis absorption is not mere summation of the absorptions from individual Cu_2S and CdS films, but suggests the added absorption as a result of Cu_2S/CdS heterojunction formed at the interface. This indicates strong coupling between CdS and Cu_2S electronic states.

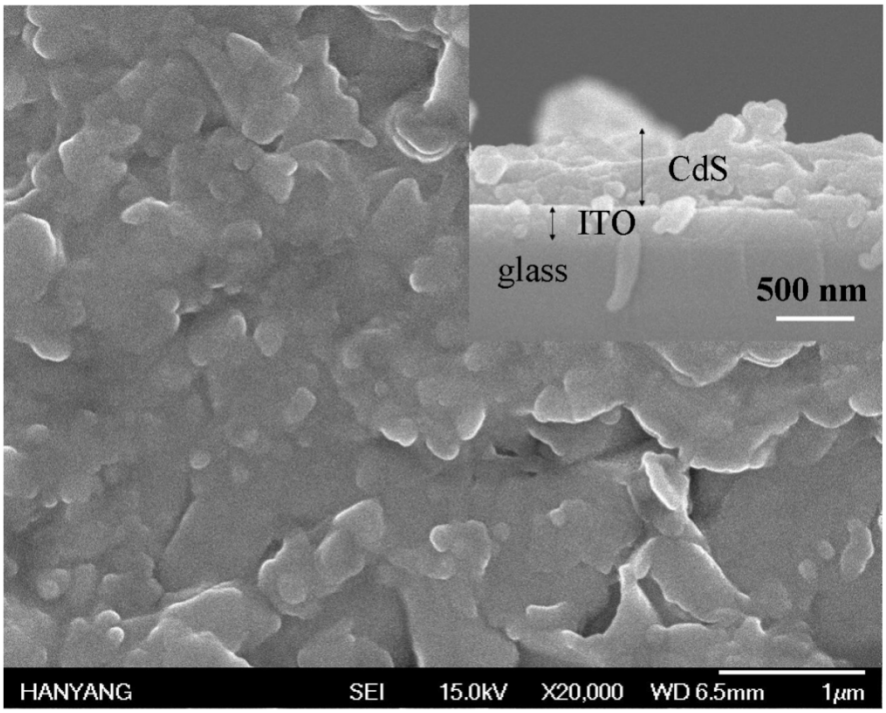

Figure S5. Representative SEM images of CdS thin-film on ITO glass substrate. Inset shows cross-sectional SEM image of the thin-film indicating the film thickness ~500 nm.

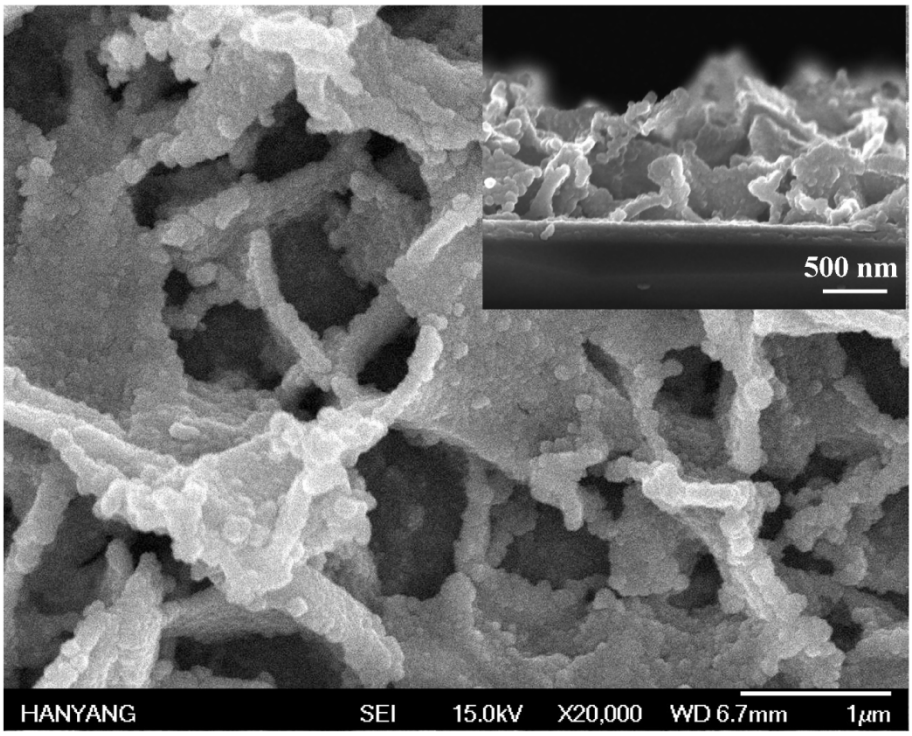

Figure S6. Representative SEM images of Cu_2S/CdS thin-film formed on ITO glass substrate with single polyethelenimine (PEI) layer used as ion protective layer during the growth of Cu_2S film leading to the formation of Cu_2S/CdS composite. The TFPT device formed using this film shows poor performance. Inset shows cross-sectional SEM image of the thin-film indicating the film thickness ~700 nm.

As seen in Fig. S6, the Cu_2S nanoparticles are observed to grow on the CdS forming several nano-heterojunctions instead of distinct Cu_2S/CdS heterojunction observed using PEI/PAA/PEI protective polyelectrolyte layers (Fig. S7 and inset). This result in damaging of the CdS layer which is reflected in the observed poor performance of the device fabricated from this film represented as device 3.

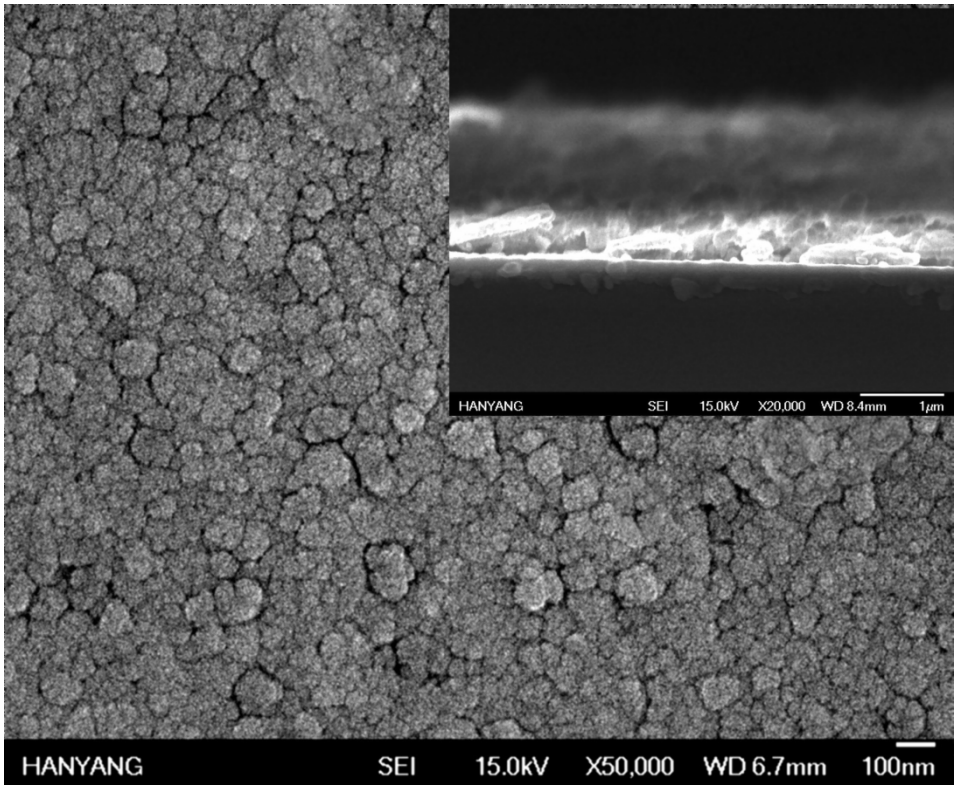

Figure S7. Representative SEM images of Cu_2S/CdS thin-film formed on ITO glass substrate with multiple $(PEI/PAA)_{1.5}$ layers used as ion protective layer during the growth of Cu_2S film leading to the formation of Cu_2S/CdS thin-film heterojunction. Inset shows cross-sectional SEM image of Cu_2S/CdS thin-film heterojunction showing two distinct layers of CdS and Cu_2S with thicknesses of ~500 and ~1000 nm, respectively.

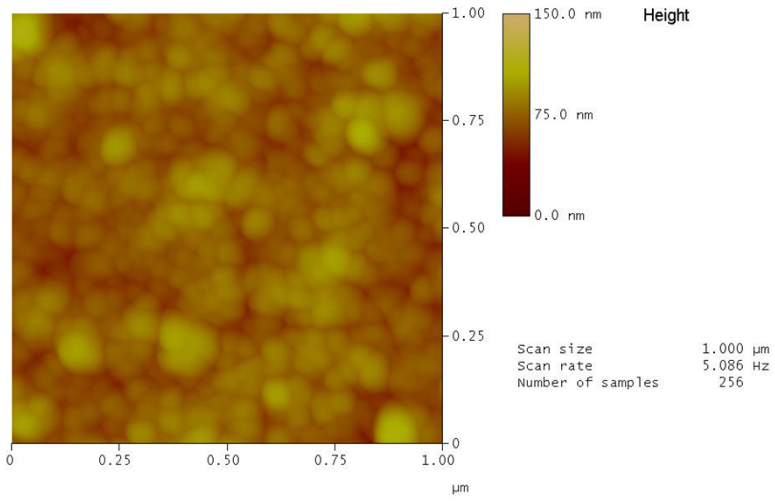

Figure S8. Representative AFM image of Cu_2S/CdS thin-film heterojunction formed on ITO glass substrate with multiple $(PEI/PAA)_{1.5}$ layers used as ion protective layer during the growth of Cu_2S film leading to the formation of Cu_2S/CdS thin-film heterojunction.

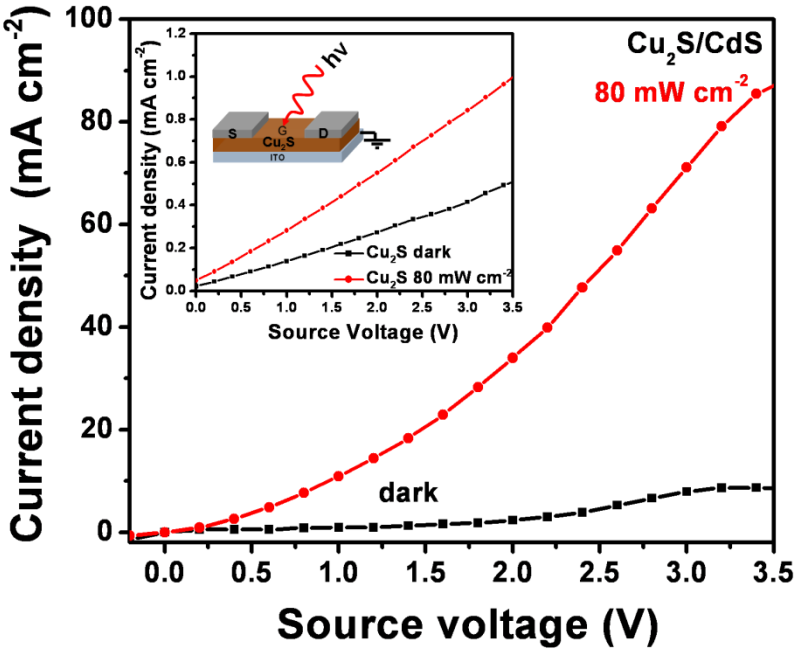

Figure S9. Comparison of the *J-V* plots obtained from TFPTs fabricated using *p*-Cu_2S/*n*-CdS thin-film heterojunction (device 1) (main figure) and individual component Cu_2S only thin-film (device 2, schematic of TFPT design shown as inset) in dark and in light (80 mW cm^{-2}) showing significant difference in photocurrent density.

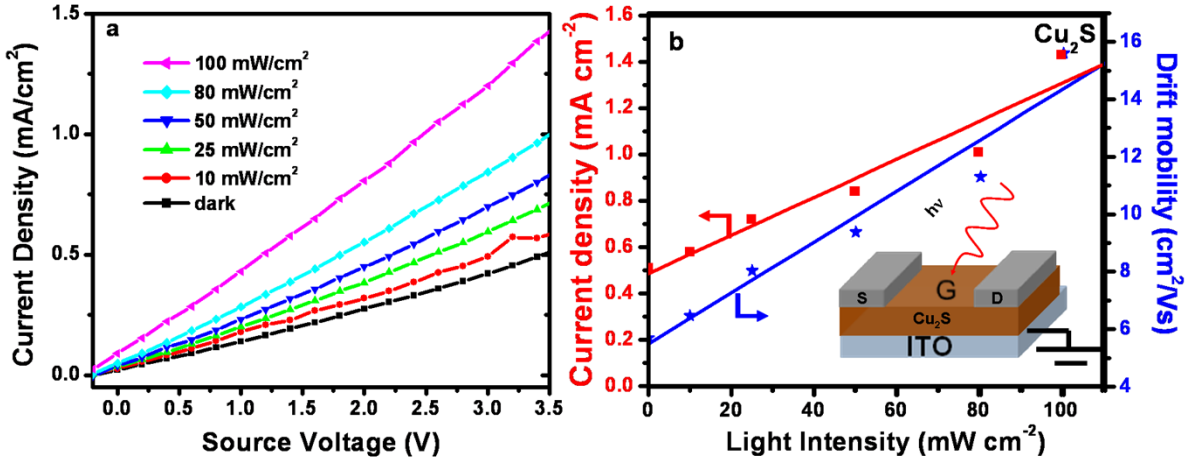

Figure S10. a, *J-V* plots in dark and with varying light intensities (10-100 mW cm^{-2}) obtained from Cu_2S only TFPT (device 2) showing significantly low photocurrent density compared to *p*-Cu_2S/*n*-CdS thin-film TFPT (device 1), but with a peculiar trend of increasing photocurrent density as a function of light intensity. **b**, Plot of photocurrent density (left y-axis scale) and drift mobility calculated from *J-V* data (right y-axis scale) at source voltage of 3.5 V as a function of light intensity (0-100 mW cm^{-2}) obtained from device 2 showing relative poor linearity. Inset shows schematic of device 2.

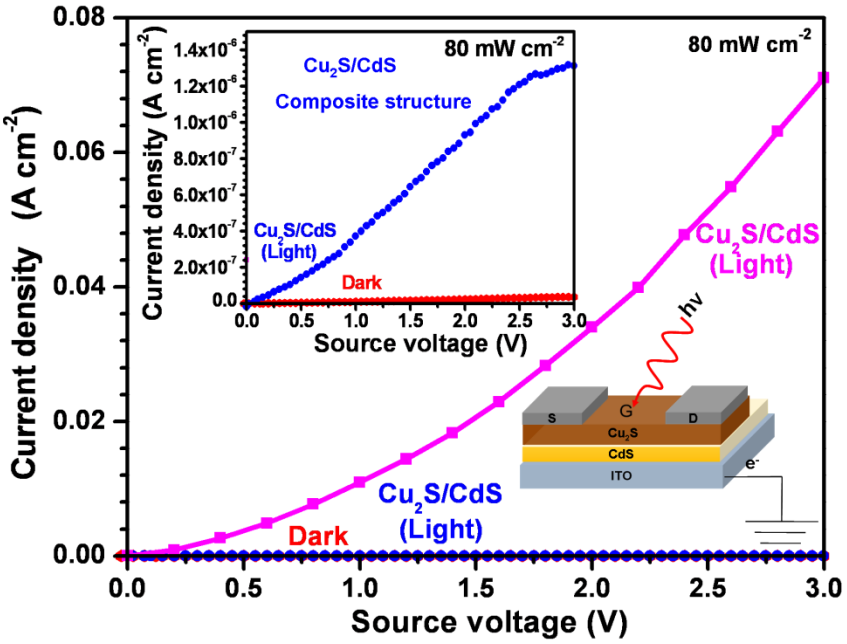

Figure S11a. Comparison of the *J-V* plots obtained from TFPTs fabricated using *p*-Cu_2S/*n*-CdS thin-film heterojunction (device 1) (main figure along with schematic of TFPT design as inset) (formed on ITO glass substrate with multiple $(PEI/PAA)_{1.5}$ layers used as ion protective polyelectrolyte layers during the growth of Cu_2S film) and Cu_2S/CdS thin-film (device 3) (plot shown as inset) (formed on ITO glass substrate with single polyethelenimine (PEI) ion protective polyelectrolyte layer used during the growth of Cu_2S film leading to the formation of Cu_2S/CdS composite structure) in dark and in light (80 mW cm^{-2}) showing significantly low photocurrent density.

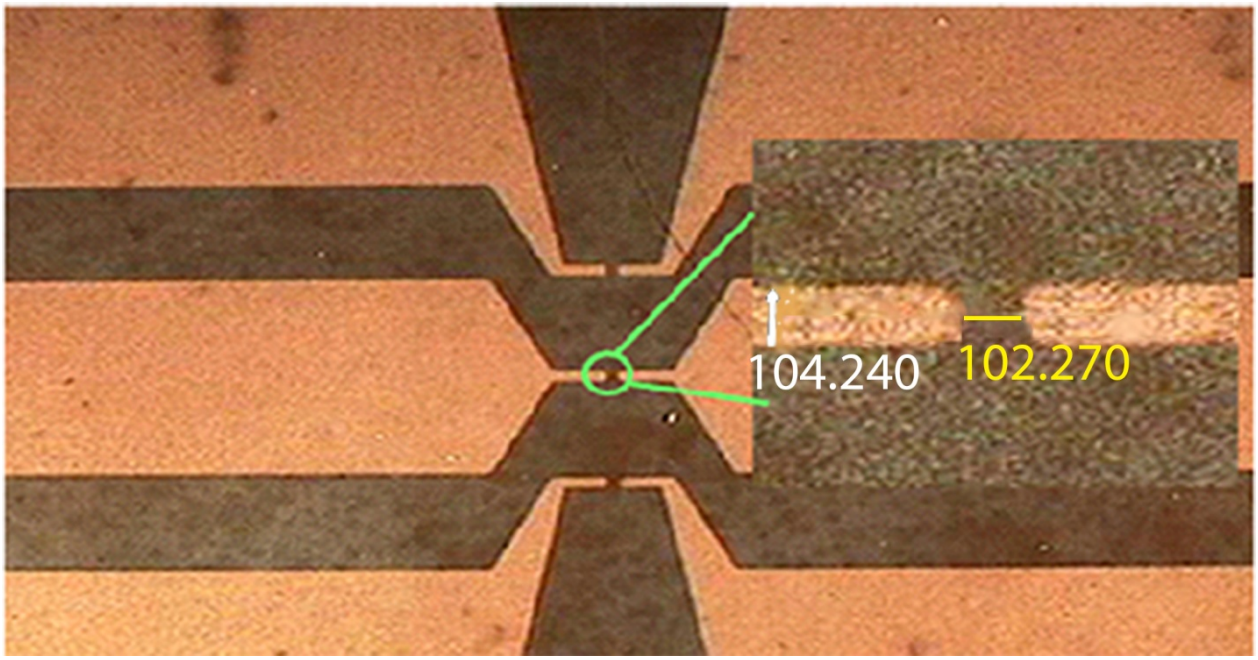

Figure 11b. The optical image of *p*-Cu_2S/*n*-CdS TFPT, when light intensity of 100 $mWcm^{-2}$ allowed to fall in between the source and drain, the generated small area (about 100 x 100 μm^2)which is known as a virtual gate(104.240 x 102.270 μm^2 ,from image) of TFPT.

Comparison of the *J-V* plots of TFPTs fabricated using Cu_2S/CdS thin-film composite (device 3) and *p*-Cu_2S/*n*-CdS thin-film heterojunction (device 1) in dark and in light shows significant difference in their profiles and the current densities therein (Fig. S11a). Both the devices show negligible photocurrent density in dark. On the other hand, the photocurrent density of the device 3 measured under the light irradiation (80 mW cm^{-2}) is observed to be four times larger than the photocurrent density noted in the dark. This is possibly due to the generation of more electrons than the holes. This can be justified from the observed film morphology in SEM images (Fig. S6) showing the dominance of porous CdS structures and several Cu_2S/CdS heterojunctions formed on the CdS nanoparticles. It is observed that larger size of the Cu_2S nanoparticles are formed in the films of device 1, than in the case of device 3, which is achieved by controlling the cation exchange reaction in between two chalcogenides. Furthermore, the current density measured from the device 1 under light irradiation (80 mW cm^{-2}) is observed to be 10,000 times higher than that in the dark or from device 3, and 100 times higher than device 2. The observed increase in photocurrent density is attributed to the uniform composition of the device and the TPFT device design, which is a unique structure, wherein *p*-Cu_2S channel is layered over the grounded *n*-CdS layer. The *n*-CdS layer effectively extracts and grounds the photo-generated electrons while blocking the holes, minimizing the carrier traps or charge

recombination in *p*-Cu_2S channel, which eventually enhances the photocurrent and drift mobility. TFPT devices were fabricated using gold metal contacts separated by 5 mm on the thin-film surfaces (Cu_2S/CdS) working as a source and drain. Fig. 11b, the optical image of *p*-Cu_2S/*n*-CdS TFPT, when light intensity of 100 mWcm^{-2} allowed to fall in between the source and drain, the generated small area (about 100 x 100 μm^2),which is known as a virtual gate of TFPT. This is further justified from the comparative data presented in Fig S12.

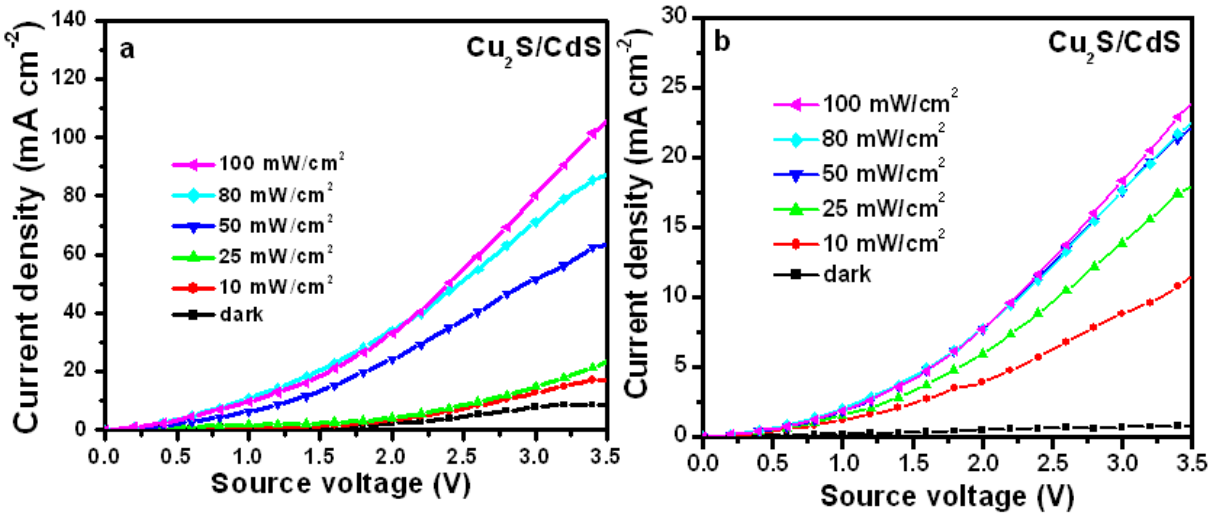

Figure S12. Comparison of the *J-V* plots obtained from TFPTs fabricated using *p*-Cu_2S/*n*-CdS thin-film heterojunction (device 1) **a**, device performance with *n*-CdS layer grounded through ITO showing peculiar trend of increase in photocurrent density as a function of light intensity and **b**, device performance without grounding *n*-CdS layer through ITO showing little increase in photocurrent density as a function of light intensity, however, only till the CdS layer is saturated with electrons (50 mW cm^{-2}). Thereafter, no increase in photocurrent density is observed.

Device 1 where the *n*-CdS layer is grounded shows significant increase in photocurrent density as a function of light intensity (Fig. S12a). On the other hand, saturation in photocurrent density is observed with increase in light intensity to 50 mW cm^{-2} and above in device where the *n*-CdS layer is not grounded (Fig. S12b). This clearly justifies the significance of the device design and the observed improvement in performance by grounding the *n*-CdS layer, which extracts and grounds the photo-generated electron enhancing the hole concentration and mobility in p-channel *p*-Cu_2S layer.

References

[1] M. K. Park, S. X. Deng, R. C. Advincula, *J. Am. Chem. Soc.* **2004**, *126*, 13723.

[2] S. S. Shiratori, M. F. Rubner, *Macromolecules* **2000**, *33*, 4213.

[3] A. A. Sagade, R. Sharma, *Sens. Actuat. B-Chem.* **2008**, *133*, 135.

[4] C. D. Wagner, W. M. Riggs, L. E. Davis, J. F. Moulder, G. E. Muilenberg, *Handbook of X-Ray Photoelectron Spectroscopy*, Perkin Elmer Corp., Eden Prairie, M.N., **1978**.

[5] J. Llanos, A. Buljan, C. Mujica, R. Ramirez, *J. Alloys Comp.* **1996**, *234*, 40.

[6] L. D. Partain, R. A. Schneider, L. F. Donaghey, P. S. McLeod, *J. Appl. Phys.* **1985**, *57*, 5056.

[7] T. J. Trentler, K. M. Hickman, S. C. Goel, A. M. Viano, P. C. Gibbons, W. E. Buhro, *Science* **1995**, *270*, 1791.

[8] O. Kulakovich, N. Strekal, A. Yaroshevich, S. Maskevich, S. Gaponenko, I. Nabiev, U. Woggon, M. Artemyev, *Nano Lett.* **2002**, *2*, 1449.